Author Manuscript

Author Manuscript

Author Manuscript

Author Manuscript

HHS Public Access

Author manuscript

Hepatology. Author manuscript; available in PMC 2024 January 01.

Published in final edited form as:

Hepatology. 2023 January 01; 77(1): 33–47. doi:10.1002/hep.32335.

Disrupted BRCA1-PALB2 Interaction Induces Tumor Immunosuppression and T-Lymphocyte Infiltration in Hepatocellular Carcinoma Through cGAS-STING Pathway

Hui Ma[1,2,3], **Zhihua Kang**[2,3], **Tzeh Keong Foo**[2,3], **Zhiyuan Shen**[2,3], **Bing Xia**[2,3]

[1]Liver Cancer Institute, Zhongshan Hospital, Fudan University, Shanghai, China

[2]Rutgers Cancer Institute of New Jersey, New Brunswick, New Jersey, USA

[3]Department of Radiation Oncology, Rutgers Robert Wood Johnson Medical School, New Brunswick, New Jersey, USA

Abstract

Background & Aim: BRCA1 and PALB2 interact with each other to promote homologous recombination and DNA double strand breaks repair. The disruption of this interaction has been reported to play a role in tumorigenesis. However, its precise function in hepatocellular carcinoma (HCC) remains poorly understood.

Approach & Results: We demonstrated that mice with disrupted BRCA1-PALB2 interaction were more susceptible to HCC than wild-type mice. HCC tumors arising from these mice showed plenty of T-lymphocyte infiltration and a better response to programmed cell death-1 (PD-1) antibody treatment. Mechanistically, disruption of the BRCA1-PALB2 interaction causes persistent high level of DNA damage in HCC cells, leading to activation of the cGAS-STING signaling pathway in both malignant hepatocytes and M1 macrophages in the tumor microenvironment. The activated cGAS-STING pathway induces PD-L1 expression via the STING-IRF3-STAT1 pathway, causing immunosuppression to facilitate tumorigenesis and tumor progression. Meanwhile, M1 macrophages with an activated cGAS-STING pathway could recruit T lymphocytes through the STING-IRF3 pathway, leading to T-lymphocyte infiltration in tumors. After normalizing immune responses by PD-1 antibody treatment, the infiltrating T lymphocytes attack tumor cells rapidly and effectively.

Conclusions: This study reveals that persistent DNA damage caused by a defective BRCA pathway induces tumor immunosuppression and T-lymphocyte infiltration in HCC through the cGAS-STING pathway, providing new insight into tumor immune microenvironment remodeling that may help improve HCC response to PD-1 antibody treatment.

Graphical Abstract

Corresponding Author: Bing Xia, Rutgers Cancer Institute of New Jersey, 195 Little Albany Street, New Brunswick, NJ 08903. Phone: 732-235-7410; Fax: 732-235-6596; xiabi@cinj.rutgers.edu.

Author contribution

H.M. and B.X. contributed to conception and design. H.M., Z.K. and F. T. K. are responsible for acquisition of data. H.M. and Z.K. analyzed and interpreted data. H.M. drafted the article. B.X. and Z. S. revised it critically for important intellectual content. All authors have read and approved the final manuscript.

Author Manuscript Author Manuscript Author Manuscript Author Manuscript

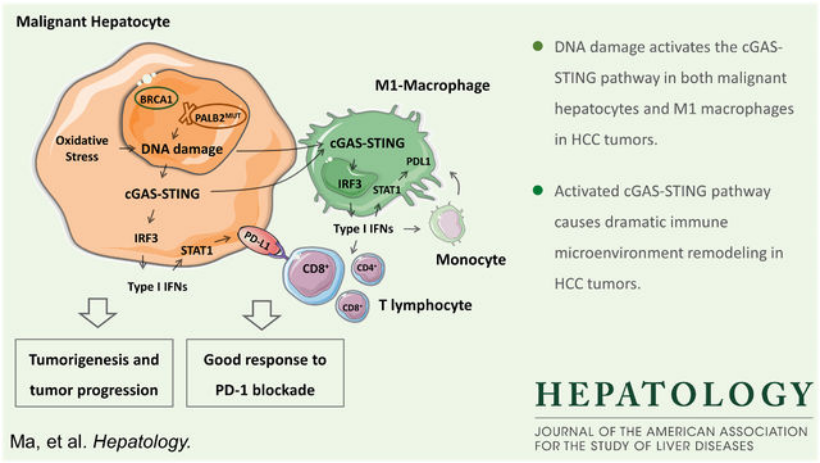

Keywords

DNA repair; DNA damage; immunotherapy; oxidative stress; M1 macrophage

Introduction

Hepatocellular carcinoma (HCC), the major primary liver cancer, is the sixth most common cancer and the fourth leading cause of cancer-related deaths worldwide [(1)]. HCC is usually diagnosed in advanced stages, resulting in limited treatment options [(2)]. Immunosuppression and immune escape play an important role in tumorigenesis and tumor progression, wherein tumor cells can express immune-inhibitory molecules innately or adaptively to evade immune attacks from the host [(3)]. Recently, immunotherapies that normalize immune responses in the tumor microenvironment, particularly through targeting the programmed cell death (PD) pathway, have been encouraging for cancer patients [(3,4)], sparking an interest in the application of immune checkpoint blockade against HCC. However, anti-PD-1 monotherapy for HCC did not reach a predetermined endpoint in two recent trials [(5,6)]. Therefore, seeking better immunotherapy strategies for HCC patients and elucidating the mechanisms is a major challenge.

The breast cancer susceptibility proteins BRCA1, BRCA2, and PALB2 (partner and localizer of BRCA2) belong to a group of molecules that participate in the repair of DNA lesions, regulation of cell cycle progression, maintenance of genomic integrity, and various transcriptional pathways[(7,8)]. PALB2, as a major BRCA2 binding partner, interacts with BRCA1 through its N-terminal coiled-coil domain, thereby recruiting BRCA2 and RAD51 recombinase to sites of DNA damage [(9,10)]. This process is critical for homologous recombination-based repair of DNA double-strand breaks (DSBs) [(9,10)]. Oxidative stress results from an imbalance between reactive oxygen species (ROS) production and removal [(11)]. As a major endogenous cause of DNA damage, this imbalance can cause oxidized lesions in DNA, which are highly damaging and carry a high mutagenic potency [(11,12)].

Stimulator of interferon genes (STING), an adaptor protein present in the endoplasmic reticulum, can be activated by cyclic GMP-AMP synthase (cGAS), which recognizes

Author Manuscript Author Manuscript Author Manuscript Author Manuscript

endogenous or exogenous double-stranded DNA (dsDNA) in the cytoplasm [13]. Activation of the cGAS-STING signaling pathway induces the release of type I interferons (IFNs) and cytokines, as well as chemokines, resulting in subsequent induction of both innate and adaptive immunity [14,15]. Recently, an increasing number of studies have revealed the critical role of STING in antitumor immunity across different types of cancer [16,17]. However, normal hepatocytes reportedly do not have a functional DNA-sensing pathway due to a lack of STING expression and cannot respond to the presence of foreign DNA in the cytosol with a type I IFN response [18]. Therefore, it is still not clear whether the cGAS-STING pathway also has the same role in HCC immunotherapy.

Previously, we generated a *Palb2* knockin mouse strain with a 3-aa mutation (LKK→AAA) in the N-terminal coiled-coil domain that abrogates BRCA1 binding [19]. Homozygous mutant mice showed increased endogenous DNA damage and oxidative stress, and following ionizing radiation they displayed accelerated lymphoma development [19,20]. In the current study, we demonstrated that these mice with disrupted BRCA1-PALB2 interaction were more susceptible to HCC than wild-type mice, and their HCC tumors displayed higher levels of DNA damage and oxidative stress. A high level of DNA damage was able to activate the cGAS-STING signaling pathway in both malignant hepatocytes and M1 macrophages in the tumor microenvironment. Moreover, these HCC tumors exhibited dramatic immune microenvironment remodeling, wherein continuous growth of the malignant mass occurred despite the infiltration of plenty of T lymphocytes, setting up a better response to anti-PD-1 treatment.

Materials and Methods

Mice

The *Palb2* (LKK-AAA)-mutant strain was described previously [19]. The strain was backcrossed to C57BL/6 background for eight generations, and then heterozygous animals were intercrossed, producing the wild-type ($Palb2^{WT}$) and homozygous mutant ($Palb2^{MUT}$) mice used in this study. All animal experiments were approved by the Institutional Animal Care and Use Committee of Rutgers University.

Cells

The human HCC cell lines MHCC97H and LM3 were established by the Liver Cancer Institute of Fudan University. The human HCC cell line Hep3B, hepatocyte-derived cell line HepG2, and the monocyte cell line THP-1 were purchased from ATCC. The human HCC cell line Huh-7 was obtained from JCRB Cell Bank. Heterozygous $Palb2^{MUT/WT}$ animals were intercrossed, and pregnant females euthanized at E.13.5 to dissect the embryos and then generate the primary mouse embryonic fibroblasts (MEFs) [19]. After genotyping, the $Palb2^{WT}$ and $Palb2^{MUT}$ MEFs (male and female) were used in this study.

Human HCC Specimens

Microarrays of tissue samples from 68 patients with histologically confirmed HCC were purchased from BioCoreUSA (DLV809a).

Author Manuscript Author Manuscript Author Manuscript Author Manuscript

Statistical Analyses

All experiments were performed at least three times unless otherwise noted. Comparisons were assessed using unpaired Student's *t* test, Pearson χ^2 test or Fisher's exact test, as appropriate. Correlations were evaluated using Pearson's *r* or Spearman's ρ when appropriate. For Kaplan-Meier survival curve, significance was estimated with log-rank test. All statistical analyses were carried out by applying SPSS (version 22.0) or GraphPad Prism (version 7.0), setting significance at $p<0.05$.

Other materials and methods, including in vivo studies and in vitro assays, are provided in the Supplementary Materials and Methods.

Results

Palb2^{MUT} Mice are More Susceptible to HCC and *Palb2*^{MUT} HCC Tumors Have High Level of T-lymphocyte Infiltration

To explore the role of BRCA1-PALB2 interaction in spontaneous tumorigenesis, *Palb2*^{WT} and *Palb2*^{MUT} mice were aged and monitored. During the study period (median, 495 days), 7 of the 26 *Palb2*^{MUT} male mice developed HCC, and the 1- and 2-year HCC tumorigenesis rates were 4.5% and 38.0%, respectively; in contrast, none of the 25 *Palb2*^{WT} male mice was found to have HCC tumors (Fig. 1A, B, C). To confirm this susceptibility, we used N-nitrosodiethylamine (DEN) to induce HCC in *Palb2*^{WT} and *Palb2*^{MUT} male mice. At 24 weeks, *Palb2*^{MUT} mice showed a high HCC incidence (80%, 4/5), whereas none of the 5 *Palb2*^{WT} mice developed this disease. At 36 weeks, although HCC tumors were found in all mice, *Palb2*^{MUT} mice had significantly more HCC tumors and larger tumor volumes than the *Palb2*^{WT} group (Fig. 1D, E, F). Interestingly, compared with HCC tumors in *Palb2*^{WT} mice, those in *Palb2*^{MUT} mice exhibited plenty of lymphocyte infiltration (Fig. 1G). To identify these lymphocytes, we performed immunohistochemistry (IHC) in serial sections of the *Palb2*^{WT} and *Palb2*^{MUT} HCC tumors. Most infiltrating cells were identified as T lymphocytes ($CD3^+$ cells); some of the T lymphocytes were cytotoxic T lymphocytes ($CD8^+$ cells), with many being Ki-67 positive, suggesting that the infiltrating T lymphocytes could proliferate and differentiate within *Palb2*^{MUT} HCC tumors (Fig. 1H, Supporting Fig. S1). These findings indicate that the mice with disrupted BRCA1-PALB2 interaction are more susceptible to HCC and that the HCC tumors with this defect display a significant increase in the level of T-lymphocyte infiltration.

Palb2^{MUT} Proliferating Cells Contain More DNA Damage, Especially Under Oxidative Stress

Because BRCA1-PALB2 interaction plays an important role in homologous recombination-based repair of DSBs, we analyzed the amount of endogenous DSBs in proliferating hepatocytes of the 4-week-old *Palb2*^{MUT} and littermate *Palb2*^{WT} mice. Phosphorylated histone H2AX (γH2AX) foci, a marker of DSBs [(9)], was counted in PCNA positive hepatocytes. The *Palb2*^{MUT} group exhibited more γH2AX foci, indicating more endogenous DNA damage in proliferating *Palb2*^{MUT} hepatocytes (Fig. 2A, Supporting Fig. S2A–C). As ROS is a major endogenous cause of DNA damage in vivo [(11)], we analyzed 8-hydroxy-2'-deoxyguanosine (8-OHdG), an oxidized derivative of deoxyguanosine formed during DNA oxidation, in the liver of growing mice and aging mice. *Palb2*^{MUT} liver tissue showed

Author Manuscript Author Manuscript Author Manuscript Author Manuscript

a stronger nuclear staining than did their *Palb2*^{WT} counterparts, indicating exposure to elevated oxidative DNA damage; as the mice aged, the oxidative DNA damage became more severe (Fig. 2B, Supporting Fig. S2D).

To explore the mechanism of DSBs formation in proliferating cells, we generated littermate MEFs. *Palb2*^{MUT} MEFs showed higher levels of ROS and higher sensitivity to H_2O_2 than *Palb2*^{WT} cells (Fig. 2C, 2D). Next, we treated these MEFs with 50 μM and 200 μM H_2O_2 to assess their response to oxidative stress. An important source of endogenous DSB generation is DNA replication stress [21]. We therefore used the DNA fiber assay to analyze replication fork progression without and with H_2O_2 treatment, which can be considered as a form of replication stress [22]. Both concentrations of H_2O_2 led to reduced replication fork speed, with *Palb2*^{MUT} MEFs showing longer replication tracts than *Palb2*^{WT} cells under the same concentration of H_2O_2 (Fig. 2E). After treatment with the single-stranded DNA (ssDNA)-specific S1 endonuclease, replication tract length in *Palb2*^{MUT} MEFs was substantially reduced, while in *Palb2*^{WT} cells it remained almost the same (Supporting Fig. S3), indicating that newly replicated DNA in the mutant cells contained much more ssDNA gaps, which could develop into DNA DSBs [23]. Indeed, more γH2AX foci were observed in *Palb2*^{MUT} MEFs under the same concentration of H_2O_2 (Fig. 2F). Both ssDNA gaps and DNA DSBs could lead to chromosome breakage [24], therefore we performed the metaphase spread assay to visualize chromosomal abnormalities. *Palb2*^{MUT} MEFs displayed a higher level of chromosome instability than littermate *Palb2*^{WT} cells under the same concentration of H_2O_2 (Fig. 2G).

Collectively, these findings constitute evidence for more DNA damage in proliferating cells with disrupted BRCA1-PALB2 interaction, especially under oxidative stress.

Palb2^{MUT} Liver Tissues Sustain More DNA Damage After DEN-Induced Acute Hepatic Stress

For initiating acute hepatic stress responses, 8-week old *Palb2*^{WT} and *Palb2*^{MUT} male mice were given a high dose of DEN (100 mg/kg; Supporting Fig. S4A) [25]. After three days, both mice groups showed significant weight loss (Supporting Fig. S4B). *Palb2*^{MUT} liver tissues exhibited more γH2AX positive and higher intensity 8-OHdG nuclear staining hepatocytes than *Palb2*^{WT} liver tissues, indicating that hepatocytes with disrupted BRCA1-PALB2 interaction sustained a higher level of DNA damage upon DEN-induced acute hepatic stress (Supporting Fig. S4C). In addition, *Palb2*^{MUT} liver tissues displayed more compensatory hepatocyte proliferation (Ki-67^{+}cells) (Supporting Fig. S4D).

The cGAS-STING Pathway is Activated in Both Malignant Hepatocytes and M1 Macrophages in *Palb2*^{MUT} HCC Tumors

Consistent with the above results, *Palb2*^{MUT} HCC tumors also had higher levels of DNA damage and oxidative stress than *Palb2*^{WT} HCC tumors (Fig. 3A, B). The cGAS-STING pathway was discovered as an important DNA-sensing machinery in innate immunity and viral defense, whose roles have been expanded to cancer with recent advances [16]. To explore the underlying mechanism of tumor immunosuppression and T-lymphocyte infiltration in *Palb2*^{MUT} HCC tumors, we assessed STING expression using

Author Manuscript Author Manuscript Author Manuscript Author Manuscript

immunofluorescence (IF) and IHC. In *Palb2*^{MUT} HCC tumors, strong positive STING expression was observed around T lymphocytes, with moderate positive expression in almost all the *Palb2*^{MUT} HCC tumor cells. In contrast, *Palb2*^{WT} HCC tumors showed very weak positive STING expression in only a few tumor cells (Fig. 3C, D). Apart from cancer-specific cGAS-STING activation, the host may harness this inflammatory pathway for tumor surveillance [16]. Moreover, macrophages, as the major antigen-presenting cells in the tumor microenvironment of HCC, are thought to recruit immune cells such as T lymphocytes and clear necrotic malignant cells through IFN signaling [26]. Thus, we also analyzed co-localization of STING, CD3, F4/80 (macrophage marker), CD11c (M1 macrophage marker), and CD206 (M2 macrophage marker) in tumor tissues using multiplex IF. From these results, cells with a strong positive STING staining were identified as the infiltrating M1 macrophages in *Palb2*^{MUT} HCC tumors (Fig. 3C). Furthermore, we assessed the downstream IRF3, STAT1, p-STAT1 and programmed death-ligand 1 (PD-L1) expression by IHC in serial sections of the two HCC tumor groups. IRF3, STAT1, and p-STAT1 (Tyr701) were all upregulated in *Palb2*^{MUT} HCC tumors compared with *Palb2*^{WT} tumors, consistent with increased STING expression (Fig. 3D). Additionally, *Palb2*^{MUT} HCC tumors displayed positive PD-L1 expression in both malignant hepatocytes and M1 Macrophages, whereas *Palb2*^{WT} tumors showed negative expression (Fig. 3D, Supporting Fig. S5). These findings indicate that cGAS-STING signaling is activated in both malignant hepatocytes and M1 macrophages in *Palb2*^{MUT} HCC tumors, presumably due to the disrupted BRCA1-PALB2 interaction. The PD-L1 expression in *Palb2*^{MUT} tumors cause immunosuppression, allowing malignant hepatocytes to evade immune attacks, and M1 macrophages infiltrate in the same area as T lymphocytes, in line with their ability to recruit lymphocytes [27].

We also assessed expression levels of PD-L1 and proteins involved in STING-IRF3-STAT1 pathway in whole HCC tumors. In addition to a higher γH2AX level, *Palb2*^{MUT} tumors showed significantly increased STING levels, and elevated IRF3, p-IRF3(Ser396), IFNα1, IFNβ1, STAT1, p-STAT1(Tyr701) and PD-L1 levels, compared with *Palb2*^{WT} tumors (Fig. 3E, F, Supporting Fig. S6A, B).

Moreover, liver tissue of 4-week-old *Palb2*^{MUT} mice, with more DNA damage, displayed elevated levels of STING, IRF3, and STAT1 expression than that of *Palb2*^{WT} counterparts (Supporting Fig. S7).

DNA Damage Induces Type I IFNs Through the cGAS-STING Pathway in Both Malignant Hepatocytes and M1 Macrophages

To determine whether STING upregulation is responsible for upregulating the IRF3 pathway in malignant hepatocytes after DNA damage, we first performed a two-step siRNA-mediated knockdown to deplete *PALB2* in HCC cells and induce DNA damage over a relatively long time yet without affecting the cell growth status (Fig. 4A, Supporting Fig. S8A). We measured cytosolic DNA using PicoGreen, a widely used fluorescent stain that selectively binds to dsDNA [28], and found that HCC cells with *PALB2* knockdown had significantly more cytosolic DNA than control cells (Fig. 4B, Supporting Fig. S8B). We next assessed γH2AX, STING, IRF3, and p-IRF3 levels in these cells. Consistent with elevated γH2AX levels, HCC cells with *PALB2* knockdown had higher levels of STING and p-IRF3 (Ser396)

Author Manuscript Author Manuscript Author Manuscript Author Manuscript

compared with control cells (Fig. 4C, Supporting Fig. S8C–E). Additionally, no significant increase in p-IRF3 (Ser396) was found in the cells when *STING* was co-depleted with *PALB2*, even with the similarly elevated γH2AX levels (Fig. 4C, Supporting Fig. S8C–E). Phosphorylated IRF3 can form a dimer and then translocate to the nucleus and induce type I IFNs [29]. Thus, we treated HCC cells and M1 macrophages with increasing concentrations of type I IFNs (IFNα1 and IFNβ). Our results demonstrated an upregulation of STAT1 and p-STAT1 (Tyr701), which has been reported as the transcription factor of PD-L1 [30], and as expected, a gradual induction of PD-L1 (Fig. 4D, Supporting Fig. S9A, B).

Furthermore, we optimized a co-culture system for in vitro studies, providing a physiologic milieu for malignant hepatocytes and M1 macrophages to interact with each other (Fig. 4E). M1 macrophages co-cultured with HCC cells carrying more DNA damage exhibited higher STING and p-IRF3 (Ser396) levels than those co-cultured with control HCC cells (Fig 4F, Supporting Fig. S10A, B). Moreover, the increase in p-IRF3 (Ser396) was not observed in M1 macrophages with *STING* depletion subjected to the same analysis (Fig. 4F, Supporting Fig. S10A, B).

Taken together, these results imply that DNA damage induces type I IFNs through the cGAS-STING pathway in both malignant hepatocytes and M1 macrophages and that type I IFNs induce PD-L1 expression in these cells through the STAT1 pathway.

Suppression of Oxidative Stress Alleviates DNA Damage and Weakens the cGAS-STING Signaling Pathway in *Palb2^{MUT}* HCC

Palb2^{MUT} mice were marked by a persistent high level of DNA damage and oxidative stress. To assess the role of oxidative stress in HCC tumorigenesis and immune microenvironment remodeling in *Palb2^{MUT}* mice, mutant males were injected with DEN at 2 weeks of age and then treated with or without reduced glutathione (GSH), which plays a major role in neutralizing ROS in vivo [31], from 4 to 36 weeks of age (Fig. 5A). *Palb2^{MUT}* mice treated with GSH (*Palb2^{MUT}*_GSH) developed fewer HCC tumors, with smaller size and volume than those without GSH treatment (*Palb2^{MUT}*_Ctrl) (Fig. 5B–D). Additionally, *Palb2^{MUT}*_GSH HCC tumors had less DNA damage and less T-lymphocyte infiltration (Fig. 5D–G, Supporting Fig. S11). Next, we assessed STING and its downstream IRF3, STAT1, and PD-L1 expression. *Palb2^{MUT}*_GSH HCC tumors displayed reduced STING, p-IRF3 (Ser396), STAT1, p-STAT1(Tyr701), and PD-L1 expression than *Palb2^{MUT}*_Ctrl HCC tumors (Fig. 5H, 5I, Supporting Fig. S12, S13). These results suggest that oxidative stress exacerbates DNA damage, and further augments cGAS-STING pathway activation in HCC tumors with disrupted BRCA1-PALB2 interaction.

Palb2^{MUT} HCC Tumors Respond Better to PD-1 Antibody Treatment

Because *Palb2^{MUT}* HCC tumor tissues contain abundant T lymphocytes and show positive PD-L1 expression, mice injected with DEN at 2 weeks old were treated with a PD-1 antibody from 32 to 36 weeks of age to assess the response of *Palb2^{WT}* and *Palb2^{MUT}* HCC tumors to immune checkpoint blockade (Fig. 6A). *Palb2^{MUT}* mice had similar number of tumors as *Palb2^{WT}* mice after PD-1 antibody treatment, but the size and volume of tumors in the mutant mice were much smaller (Fig. 6B, C), which was the opposite to the results

Author Manuscript Author Manuscript Author Manuscript Author Manuscript

obtained in mice untreated with anti-PD-1 (Fig. 1D, E). Notably, although *Palb2*^{MUT} tumors had more CD8 positive T lymphocyte infiltration than *Palb2*^{WT} tumors, no significant difference in tumor cell death was observed between the two groups untreated with PD-1 antibody (Fig. 6D, Supporting Fig. S14). However, after using PD-1 antibody to normalize immune responses, *Palb2*^{MUT} tumors had dramatically more HCC cell death than *Palb2*^{WT} tumors (Fig. 6D). These findings indicate that HCC tumors with disrupted BRCA1-PALB2 interaction have a better response to PD-1 antibody treatment than wild-type tumors.

DNA Damage Is Associated with STING Expression in Human HCC Tissues

Using tissue microarrays, IHC was performed to gauge γH2AX, 8-OHdG, and STING levels in tumor specimens from 68 patients with HCC. Figure 7A shows representative images of low expression (case 49) and high expression (case 69). The H-score was used to denote the level of the target expression, and statistical analysis revealed a positive correlation between γH2AX and STING levels (R^2=0.485; $p<0.001$), as well as between 8-OHdG and STING levels (R^2=0.448; $p<0.001$; Fig. 7B).

STING Expression Is Associated with Tumor Immunosuppression and T-Lymphocyte Infiltration in Human HCC Tissues

Gene expression analysis using The Cancer Genome Atlas (TCGA) database showed a positive correlation between *STING (TMEM173)* and *STAT1* expression (R^2=0.110; $p<0.001$) and also a positive correlation between *STING* and *PD-L1 (CD274)* expression in 371 HCC tissues (R^2=0.169; $p<0.001$; Fig. 7C). Given the association of *STING* expression with *PD-L1* expression, we next investigated the correlation between the expression of *STING*, *IRF3* and *STAT1* and those of 44 common immune checkpoint genes. Interestingly, we found that in HCC tissues, *STING* expression was correlated with 42 of the checkpoint markers, *IRF3* with 35, and *STAT1* with 42 (Fig. 7D). In addition, we studied whether *STING* expression was correlated with the level of immune infiltration in human HCC tissues. Our results showed that *STING* expression was significantly correlated with infiltrating immune cells, including $CD4^+$ T cells, $CD8^+$ T cells, and macrophages, estimated by Tumor Immune Estimation Resource (TIMER) [32] (Fig. 7E). Collectively, these results suggest that STING expression plays a vital role in tumor immunosuppression and T-lymphocyte infiltration in human HCC tissues.

Discussion

As an opportunity for a cure, immune checkpoint blockade therapy has revolutionized cancer treatment. In practice, however, most HCC patients have shown a lack of response to monotherapy, underscoring the pressing need to clarify the mechanism of action for optimal patient selection and immunotherapy strategy [33,34].

In the present study, we found that mice with disrupted BRCA1-PALB2 interaction are more susceptible to HCC than wild-type mice and that HCC tumors arising from the mutant mice displayed high levels of DNA damage and oxidative stress. Interestingly, these tumors showed activation of the cGAS-STING signaling pathway in both malignant hepatocytes and M1 macrophages in the tumor microenvironment (Fig. 7F). The activated

Author Manuscript Author Manuscript Author Manuscript Author Manuscript

cGAS-STING pathway in HCC tumors induced PD-L1 expression through the STING-IRF3-STAT1 pathway causing immunosuppression, while in M1 macrophages it also promoted T-lymphocyte infiltration through the STING-IRF3 pathway. Notably, such HCC tumors with both immunosuppression and T-lymphocyte infiltration exhibited a better response to PD-1 antibody treatment. This newly described chain of events represents a distinct path of HCC tumorigenesis and progression from DNA damage to tumor immune microenvironment remodeling. As such, HCC tumors with DNA repair defects may be sensitive to immune checkpoint inhibitors, and thus, treatments that combine these inhibitors with therapeutic methods which cause persistent DNA damage, are promising for HCC treatment.

Germline mutations in *BRCA1, BRCA2 or PALB2* may cause increased risks of developing human breast, ovarian, pancreatic, prostate, and stomach cancers [35,36]. To our knowledge, our results represent the first evidence that mice with a defect in the BRCA1-PALB2-BRCA2 pathway are more susceptible to HCC in both spontaneous and carcinogen-induced settings. This will help us to understand more fully the importance of the BRCA pathway in HCC tumorigenesis and treatment.

DNA damage resulting from various sources has been shown to increase intracellular levels of ROS through γH2AX-mediated activation of the Nox1-Rac1 complex [37]. In turn, ROS has been reported to directly induce DNA damage through oxidizing nucleoside bases, potentially leading to G-T or G-A transversions [12]. Besides homologous recombination-based repair, the BRCA pathway is also required for the transcription-coupled repair of the oxidative DNA damage site, which may lead to either transcription blockage or mutagenic bypass if not be repaired [12,38]. Therefore, in our model, due to a DNA repair defect, HCC cells with disrupted BRCA1-PALB2 interaction displayed high levels of DNA damage and oxidative stress. Because these two factors promote each other, DNA damage persists and becomes worse over time.

Recent studies have revealed that the cGAS-STING pathway occupies a central role in antitumor immune responses across different types of cancer with DNA damage response deficiency, including breast, ovarian, prostate, and lung cancers [39]. Our data provide more comprehensive evidences about the role of the cGAS-STING pathway in HCC with chronically elevated DNA damage, from tumorigenesis to tumor immunotherapy response. Importantly, the pathway plays a dual role simultaneously. Tumor DNA or tumor cGAMP can activate the cGAS-STING pathway in antigen-presenting cells [16], such as M1 macrophages, possibly recruiting T lymphocytes to the area where tumor DNA or cGAMP has been sensed and promoting T-lymphocyte proliferation and differentiation within tumor tissues. On the other hand, malignant hepatocytes with activated cGAS-STING pathway express PD-L1 causing immunosuppression to facilitate tumorigenesis and tumor progression. As a result, when these tumors are treated with PD-1 antibody to normalize immune responses, the infiltrating T lymphocytes were able to attack tumor cells rapidly and effectively.

Notably, normal hepatocytes reportedly do not have a functional DNA-sensing pathway due to the lack of STING expression [18], and the cGAS-STING pathway is activated in

Author Manuscript Author Manuscript Author Manuscript Author Manuscript

nonparenchymal cells but not malignant hepatocytes in HCC [40]. Consistent with these results, our data showed that both wild-type hepatocytes and HCC cells displayed no or very low STING expression, whereas transformed hepatocytes and HCC cells with persistent DNA damage showed higher STING expression. In line with this, our human HCC analyses showed a positive correlation between DNA damage and STING expression. In practice, HCC frequently arises in the context of chronic injury and inflammation that promote DNA damage [41]. Several types of DNA damage caused by defects in DNA repair mechanisms also have been implicated in HCC, such as DSBs, stalled DNA replication fork and base mismatches [42,43]. Moreover, previous studies have uncovered correlations between HCC and aberrations of DNA damage response proteins such as the ATM kinase [42]. In addition, standard treatments for HCC, including chemotherapy and radiotherapy, can cause DNA damage in HCC tumors. Therefore, the role of DNA damage and the cGAS-STING pathway in antitumor immunity may be generalized to a considerable number of HCC patients. However, more clinical evidence is still needed to support these results.

Collectively, the present data show that persistent DNA damage caused by a defective BRCA pathway induces tumor immunosuppression and T-lymphocyte infiltration in HCC through the cGAS-STING pathway. Our findings provide new insights into DNA damage and the cGAS-STING pathway activation in HCC, which may be harnessed to enhance the response to immune checkpoint blockade in patients with HCC.

Supplementary Material

Refer to Web version on PubMed Central for supplementary material.

Acknowledgement

We thank Dr. Chen Liu (Department of Pathology, Yale Medical School, New Haven, USA) for pathological diagnosis.

Financial Support:

This work was supported by the National Cancer Institute (R01CA138804 and P01CA250957-9485 to B. Xia).

List of Abbreviations:

cGAS	cyclic GMP-AMP synthase
DEN	N-Nitrosodiethylamine
DSBs	double-strand breaks
dsDNA	double-stranded DNA
GSH	glutathione reduced
HCC	hepatocellular carcinoma
IFN	interferon
MEFs	mouse embryonic fibroblasts

Author Manuscript Author Manuscript Author Manuscript Author Manuscript

PD	program cell death
ROS	reactive oxygen species
ssDNA	single-stranded DNA
STING	stimulator of interferon genes
TCGA	The Cancer Genome Atlas
TIMER	Tumor Immune Estimation Resource

Reference

1). Sung H, Ferlay J, Siegel RL, Laversanne M, Soerjomataram I, Jemal A, et al. Global cancer statistics 2020: GLOBOCAN estimates of incidence and mortality worldwide for 36 cancers in 185 countries. CA Cancer J Clin 2021; 71: 209–249. [PubMed: 33538338]

2). Llovet JM, Kelley RK, Villanueva A, Singal AG, Pikarsky E, Roayaie S, et al. Hepatocellular carcinoma. Nat Rev Dis Prim 2021; 7: 6. [PubMed: 33479224]

3). Smyth MJ, Ngiow SF, Ribas A, Teng MWL. Combination cancer immunotherapies tailored to the tumour microenvironment. Nat Rev Clin Oncol 2016; 13: 143–158. [PubMed: 26598942]

4). Hargadon KM, Johnson CE, Williams CJ. Immune checkpoint blockade therapy for cancer: an overview of FDA-approved immune checkpoint inhibitors. Int Immunopharmacol 2018; 62: 29–39. [PubMed: 29990692]

5). Finn RS, Ryoo BY, Merle P, Kudo M, Bouattour M, Lim HY, et al. Pembrolizumab as second-line therapy in patients with advanced hepatocellular carcinoma in KEYNOTE-240: a randomized, double-blind, phase III trial. J Clin Oncol 2020; 38: 193–202. [PubMed: 31790344]

6). El-Khoueiry AB, Sangro B, Yau T, Crocenzi TS, Kudo M, Hsu CN, et al. Nivolumab in patients with advanced hepatocellular carcinoma (CheckMate 040): an open-label, non-comparative, phase 1/2 dose escalation and expansion trial. Lancet 2017; 389: 2492–2502. [PubMed: 28434648]

7). Rosen EM, Fan SJ, Pestell RG, Goldberg ID. BRCA1 gene in breast cancer. J Cell Physiol 2003; 196: 19–41. [PubMed: 12767038]

8). Xia B, Sheng Q, Nakanishi K, Ohashi A, Wu J, Christ N, et al. Control of BRCA2 cellular and clinical functions by a nuclear partner, PALB2. Mol Cell 2006; 22: 719–29. [PubMed: 16793542]

9). Sy SM, Huen MS, Chen J. PALB2 is an integral component of the BRCA complex required for homologous recombination repair. Proc Natl Acad Sci U S A 2009; 106: 7155–60. [PubMed: 19369211]

10). Zhang F, Ma J, Wu J, Ye L, Cai H, Xia B, et al. PALB2 links BRCA1 and BRCA2 in the DNA-damage response. Curr Biol 2009; 19: 524–529. [PubMed: 19268590]

11). Srinivas US, Tan BWQ, Vellayappan BA, Jeyasekharan AD. ROS and the DNA damage response in cancer. Redox Biol 2019; 25: 101084. [PubMed: 30612957]

12). Salehi F, Behboudi H, Kavoosi G, Ardestani SK. Oxidative DNA damage induced by ROS-modulating agents with the ability to target DNA: A comparison of the biological characteristics of citrus pectin and apple pectin. Sci Rep 2018; 8: 13902. [PubMed: 30224635]

13). Sun L, Wu J, Du F, Chen X, Chen ZJ. Cyclic GMP-AMP synthase is a cytosolic DNA sensor that activates the type I interferon pathway. Science 2013; 339: 786–791. [PubMed: 23258413]

14). Li T, Chen ZJ. The cGAS-cGAMP-STING pathway connects DNA damage to inflammation, senescence, and cancer. J Exp Med 2018; 215: 1287–1299. [PubMed: 29622565]

15). Lippert TP, Greenberg RA. The abscopal effect: a sense of DNA damage is in the air. J Clin Invest 2021; 131: e148274. [PubMed: 33938453]

16). Kwon J, Bakhoum SF. The cytosolic DNA-sensing cGAS-STING pathway in cancer. Cancer Discov 2020; 10: 26–39. [PubMed: 31852718]

Author Manuscript Author Manuscript Author Manuscript Author Manuscript

17). Zheng JY, Mo JL, Zhu T, Zhuo W, Yi YN, Hu S, et al. Comprehensive elaboration of the cGAS-STING signaling axis in cancer development and immunotherapy. Mol Cancer 2020; 19: 133. [PubMed: 32854711]

18). Thomsen MK, Nandakumar R, Stadler D, Malo A, Valls RM, Wang F, et al. Lack of immunological DNA sensing in hepatocytes facilitates hepatitis B virus infection. Hepatology 2016; 64: 746–759. [PubMed: 27312012]

19). Simhadri S, Peterson S, Patel DS, Huo YY, Cai H, Bowman-Colin C, et al. Male fertility defect associated with disrupted BRCA1-PALB2 interaction in mice. J Biol Chem 2014; 289: 24617–24629. [PubMed: 25016020]

20). Mahdi AH, Huo Y, Tan Y, Simhadri S, Vincelli G, Gao J, et al. Evidence of Intertissue Differences in the DNA Damage Response and the Pro-oncogenic Role of NF-kB in Mice with Disengaged BRCA1–PALB2 Interaction. Cancer Res 2018; 78: 3969–3981. [PubMed: 29739757]

21). Kotsantis P, Petermann E, Boulton SJ. Mechanisms of oncogene-induced replication stress: jigsaw falling into place. Cancer Discov 2018; 8: 537–555. [PubMed: 29653955]

22). Kang Z, Fu P, Alcivar AL, Fu H, Redon C, Foo TK, et al. BRCA2 associates with MCM10 to suppress PRIMPOL-mediated repriming and single-stranded gap formation after DNA damage. Nat Commun 2021; 12: 5966. [PubMed: 34645815]

23). Panzarino NJ, Krais JJ, Cong K, Peng M, Mosqueda M, Nayak SU, et al. Replication gaps underlie BRCA deficiency and therapy response. Cancer Res 2021; 81: 1388–1397. [PubMed: 33184108]

24). Guan JH, Lu CZ, Jin QH, Lu HM, Chen X, Tian L, et al. MLH1 deficiency-triggered DNA hyperexcision by exonuclease 1 activates the cGAS-STING pathway. Cancer Cell 2021; 39: 109–121. [PubMed: 33338427]

25). Ge CM, Vilfranc CL, Che LX, Pandita RK, Hambarde S, Andreassen PR, et al. The BRUCE-ATR signaling axis is required for accurate DNA replication and suppression of liver cancer development. Hepatology 2019; 69: 2608–2622. [PubMed: 30693543]

26). Liu JY, Geng XF, Hou JX, Wu GS. New insights into M1/M2 macrophages: key modulators in cancer progression. Cancer Cell Int 2021; 21: 389. [PubMed: 34289846]

27). Lam KC, Araya RE, Huang A, Chen Q, Di Modica M, Rodrigues RR, et al. Microbiota triggers STING-type I IFN-dependent monocyte reprogramming of the tumor microenvironment. Cell 2021; 184: 5338–5356. [PubMed: 34624222]

28). Shen YJ, Le Bert N, Chitre AA, Koo CX, Nga XH, Ho SSW, et al. Genome-derived cytosolic DNA mediates type I interferon-dependent rejection of B cell lymphoma cells. Cell Rep 2015; 11: 460–473. [PubMed: 25865892]

29). Yum S, Li MH, Fang Y, Chen ZJ. TBK1 recruitment to STING activates both IRF3 and NF-kappa B that mediate immune defense against tumors and viral infections. Proc Natl Acad Sci 2021; 118: e2100225118. [PubMed: 33785602]

30). Kharma B, Baba T, Matsumura N, Kang HS, Hamanishi J, Murakami R, et al. STAT1 drives tumor progression in serous papillary endometrial cancer. Cancer Res 2014; 74: 6519–6530. [PubMed: 25267067]

31). Aw TY, Wierzbicka G, Jones DP. Oral glutathione increases tissue glutathione in vivo. Chem Biol Interact 1991; 80: 89–97. [PubMed: 1913980]

32). Li Taiwen, Fan Jingyu, Wang Binbin, Traugh Nicole, Chen Qianming, Liu Jun S., et al. TIMER: A web server for comprehensive analysis of tumor-infiltrating immune cells. Cancer Res 2017; 77: e108–e110. [PubMed: 29092952]

33). Worns MA, Galle PR. Immune oncology in hepatocellular carcinoma-hype and hope. Lancet 2017; 389: 2448–2449. [PubMed: 28434649]

34). Singh A, Beechinor RJ, Huynh JC, Li DN, Dayyani F, Valerin JB, et al. Immunotherapy updates in advanced hepatocellular carcinoma. Cancers 2021; 13: 2164. [PubMed: 33946408]

35). Wu H, Wu X, Liang Z. Impact of germline and somatic BRCA1/2 mutations: tumor spectrum and detection platforms. Gene Ther 2017; 24: 601–609. [PubMed: 28771233]

36). Nepomuceno TC, Carvalho MA, Rodrigue A, Simard J, Masson JY, Monteiro ANA. PALB2 variants: protein domains and cancer susceptibility. Trends Cancer 2020; 7: 188–197. [PubMed: 33139182]

Author Manuscript Author Manuscript Author Manuscript Author Manuscript

37). Kang MA, So EY, Simons AL, Spitz DR, Ouchi T. DNA damage induces reactive oxygen species generation through the H2AX-Nox1/Rac1 pathway. Cell Death Dis 2012; 3: 1–8.

38). Le Page F, Randrianarison V, Marot D, Cabannes J, Perricaudet M, Feunteun J,et al. BRCA1 and BRCA2 are necessary for the transcription-coupled repair of the oxidative 8-oxoguanine lesion in human cells. Cancer Res 2000; 60: 5548–5552. [PubMed: 11034101]

39). Le Naour J, Zitvogel L, Galluzzi L, Vacchelli E, Kroemer G. Trial watch: STING agonists in cancer therapy. Oncoimmunology 2020; 9: 1777624. [PubMed: 32934881]

40). Thomsen MK, Skouboe MK, Boularan C, Vernejoul F, Lioux T, Leknes SL, et al. The cGAS-STING pathway is a therapeutic target in a preclinical model of hepatocellular carcinoma. Oncogene 2020; 39: 1652–1664. [PubMed: 31740782]

41). Buitrago-Molina, Marhenke S, Longerich T, Sharma AD, Boukouris AE, Geffers R, et al. The degree of liver injury determines the role of p21 in liver regeneration and hepatocarcinogenesis in mice. Hepatology 2013; 58: 1143–1152. [PubMed: 23526443]

42). Yang SF, Chang CW, Wei RJ, Shiue YL, Wang SN, Yeh YT. Involvement of DNA damage response pathways in hepatocellular carcinoma. Biomed Res Int 2014; 2014: 153867. [PubMed: 24877058]

43). Gao Q, Zhu HW, Dong LQ, Shi WW, Chen R, Song ZJ, et al. Integrated proteogenomic characterization of HBV-related hepatocellular carcinoma. Cell 2019; 179: 561–577. [PubMed: 31585088]

Author Manuscript Author Manuscript Author Manuscript Author Manuscript

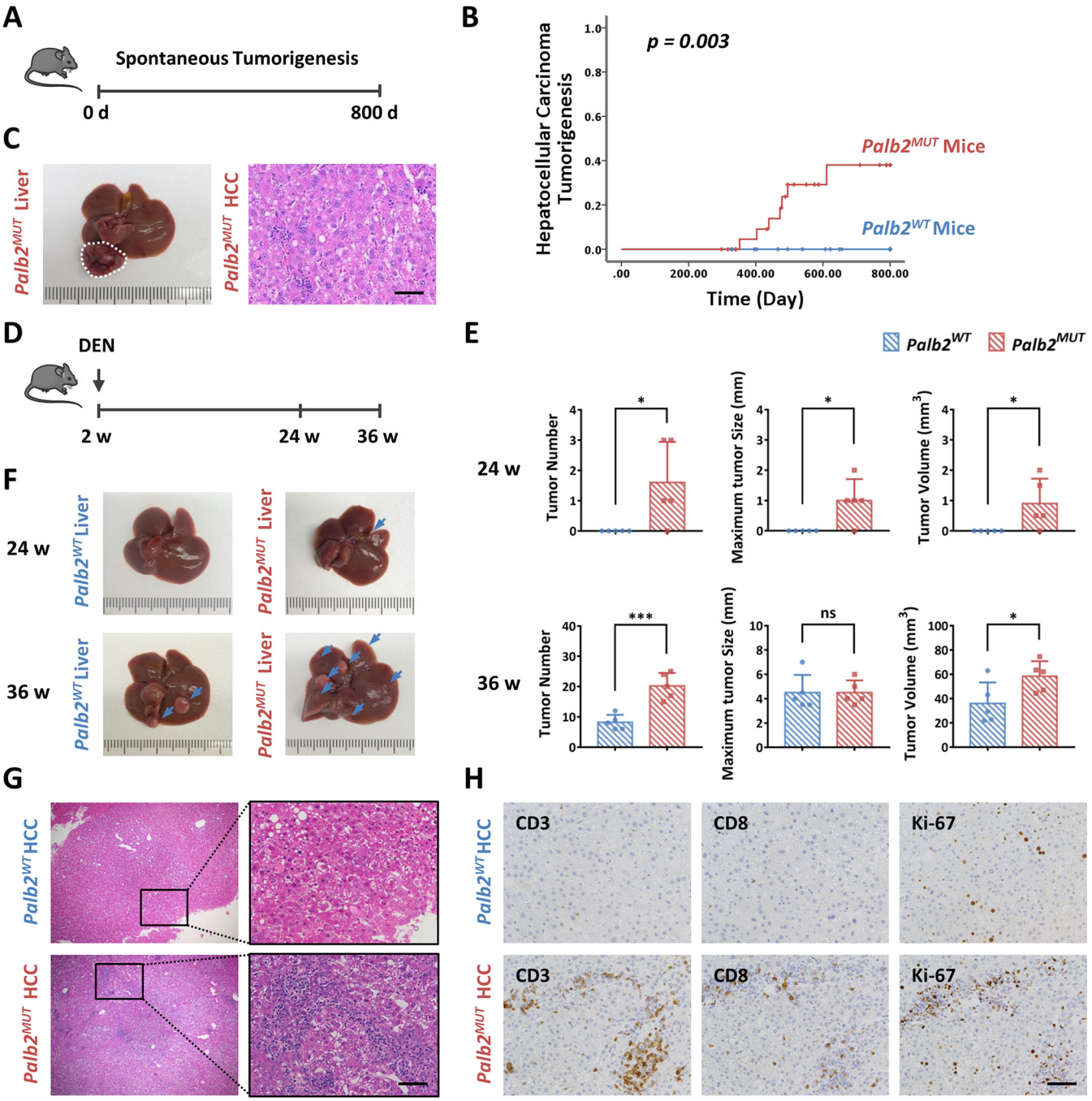

Figure 1. *Palb2*^{MUT} mice are more susceptible to HCC and *Palb2*^{MUT} HCC tumors have increased T-lymphocyte infiltration.

(A) Schematic diagram showing the spontaneous tumorigenesis model in *Palb2*^{WT} (n=25 males) and *Palb2*^{MUT} (n=26 males) mice.

(B) Kaplan-Meier analysis of HCC tumorigenesis for the *Palb2*^{WT} and *Palb2*^{MUT} mice.

(C) Representative gross appearance image of *Palb2*^{MUT} mouse liver, and H&E image of the HCC tumor (liver tumor in white circle; scale bar, 50 μm).

(D) Schematic diagram showing the DEN-induced HCC tumorigenesis model in *Palb2*^{WT} and *Palb2*^{MUT} mice (n = 5 males per group).

Author Manuscript Author Manuscript Author Manuscript Author Manuscript

(E) Quantification of tumor number, maximum size, and total volume in *Palb2*^{WT} and *Palb2*^{MUT} mouse livers after DEN treatment. *Palb2*^{MUT} mouse livers had more tumors and larger tumor volume.
(F) Representative gross appearance images of the *Palb2*^{WT} and *Palb2*^{MUT} mouse livers after DEN treatment (arrows point to tumors).
(G) Representative H&E images showing increased lymphocyte infiltration in *Palb2*^{MUT} HCC tumors (scale bar, 50 μm).
(H) Representative IHC images showing more CD3, CD8, and Ki-67 positive lymphocytes infiltrating in *Palb2*^{MUT} HCC tumors (scale bar, 50 μm).
(*$*p < 0.05$, $***p < 0.001$*; mean ± SD)

Author Manuscript
Author Manuscript
Author Manuscript
Author Manuscript

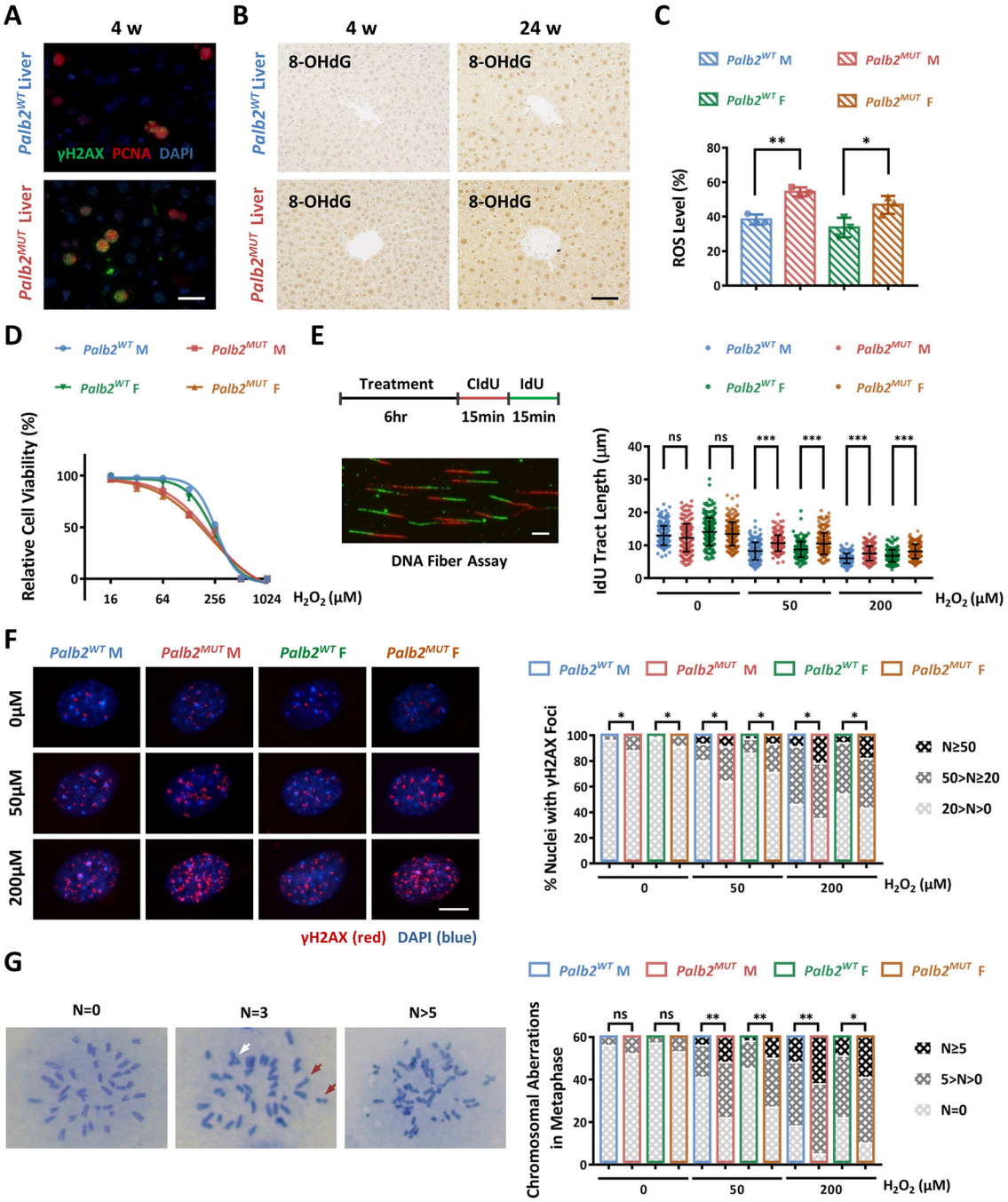

Figure 2. *Palb2*^{MUT} proliferating cells exhibit more DNA damage especially under oxidative stress.

(A) Representative IF images showing PCNA positive nuclei with more γH2AX foci in 4-week-old *Palb2*^{MUT} mouse liver (scale bar, 20 μm).

(B) Representative IHC images showing stronger 8-OHdG nuclear staining in 4-week old and 24-week-old *Palb2*^{MUT} mouse liver (scale bar, 50 μm).

(C) Quantification of ROS levels in *Palb2*^{WT} and *Palb2*^{MUT} MEFs. The DCFH-DA fluorescence intensity was measured by flow cytometry.

(D) Sensitivity of *Palb2*^{WT} and *Palb2*^{MUT} MEFs to H_2O_2.

Author Manuscript Author Manuscript Author Manuscript Author Manuscript

(E) Left panel: labeling scheme and a representative image of the DNA fiber assay (scale bar, 10μm). Right panel: lengths of IdU-labeled replication tracts in *Palb2*^{WT} and *Palb2*^{MUT} MEFs with H_2O_2 (0, 50, and 200 μM) treatment.
(F) Representative IF images (left) and quantification (right) showing more γH2AX foci in *Palb2*^{MUT} MEFs with H_2O_2 (0, 50, and 200 μM) treatment (N, foci count; scale bar, 5μm).
(G) Representative images of mitotic spreads (left) and quantification of chromosomal aberration (right) in *Palb2*^{WT} and *Palb2*^{MUT} MEFs with H_2O_2 (0, 50, and 200 μM) treatment (red arrow, chromatid break; white arrow, radial chromosome; N, the number of chromosomal aberration).
(*Palb2*^{WT}, littermate control; M, male; F, female; *$p < 0.05$, **$p < 0.01$, ***$p < 0.001$; mean ± SD)

Author Manuscript Author Manuscript Author Manuscript Author Manuscript

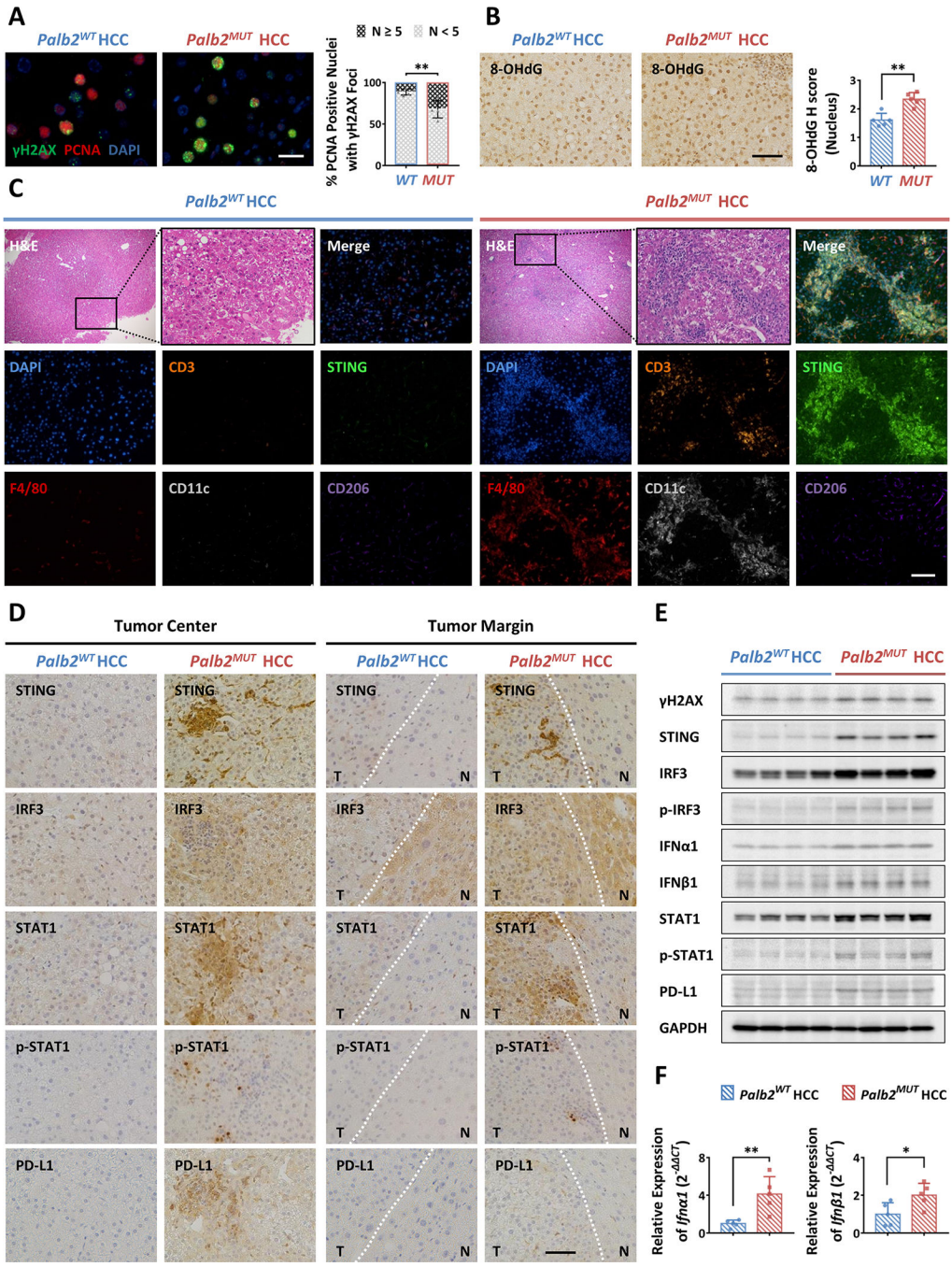

Figure 3. The cGAS-STING pathway is activated in both malignant hepatocytes and M1 macrophages in *Palb2*^{MUT} HCC tumors.

(A) Representative IF images (left) and quantification (right) showing PCNA positive nuclei with more γH2AX foci in *Palb2*^{MUT} HCC tumors (N, foci count; scale bar, 20 μm).

(B) Representative IHC images (left) and quantification using H score (right) showing stronger 8-OHdG nuclear staining in *Palb2*^{MUT} HCC tumors (scale bar, 50 μm).

(C) H&E staining and co-localization of STING, CD3, F4/80, CD11c, and CD206 in *Palb2*^{WT} and *Palb2*^{MUT} HCC tumors using multiplex IF; *Palb2*^{MUT} HCC tumors had

Author Manuscript Author Manuscript Author Manuscript Author Manuscript

upregulated STING expression in both malignant hepatocytes and M1 macrophages (scale bar, 50 μm).

(D) Representative IHC images of tumor center and tumor margin showing higher STING, IRF3, STAT1, and p-STAT1 levels, and positive PD-L1 expression in *Palb2*^{MUT} HCC tumors (T, HCC tumor; N, adjacent normal liver tissue; scale bar, 50 μm).

(E) Western blots showing increased γH2AX, STING, IRF3, p-IRF3, IFNα1, IFNβ1, STAT1, p-STAT1 and PD-L1 protein levels in *Palb2*^{MUT} HCC tumors.

(F) qRT-PCR analysis showing elevated *Ifnα1* and *Ifnβ1* mRNA levels in *Palb2*^{MUT} HCC tumors.

(*$p < 0.05$, **$p < 0.01$; mean ± SD)

Author Manuscript Author Manuscript Author Manuscript Author Manuscript

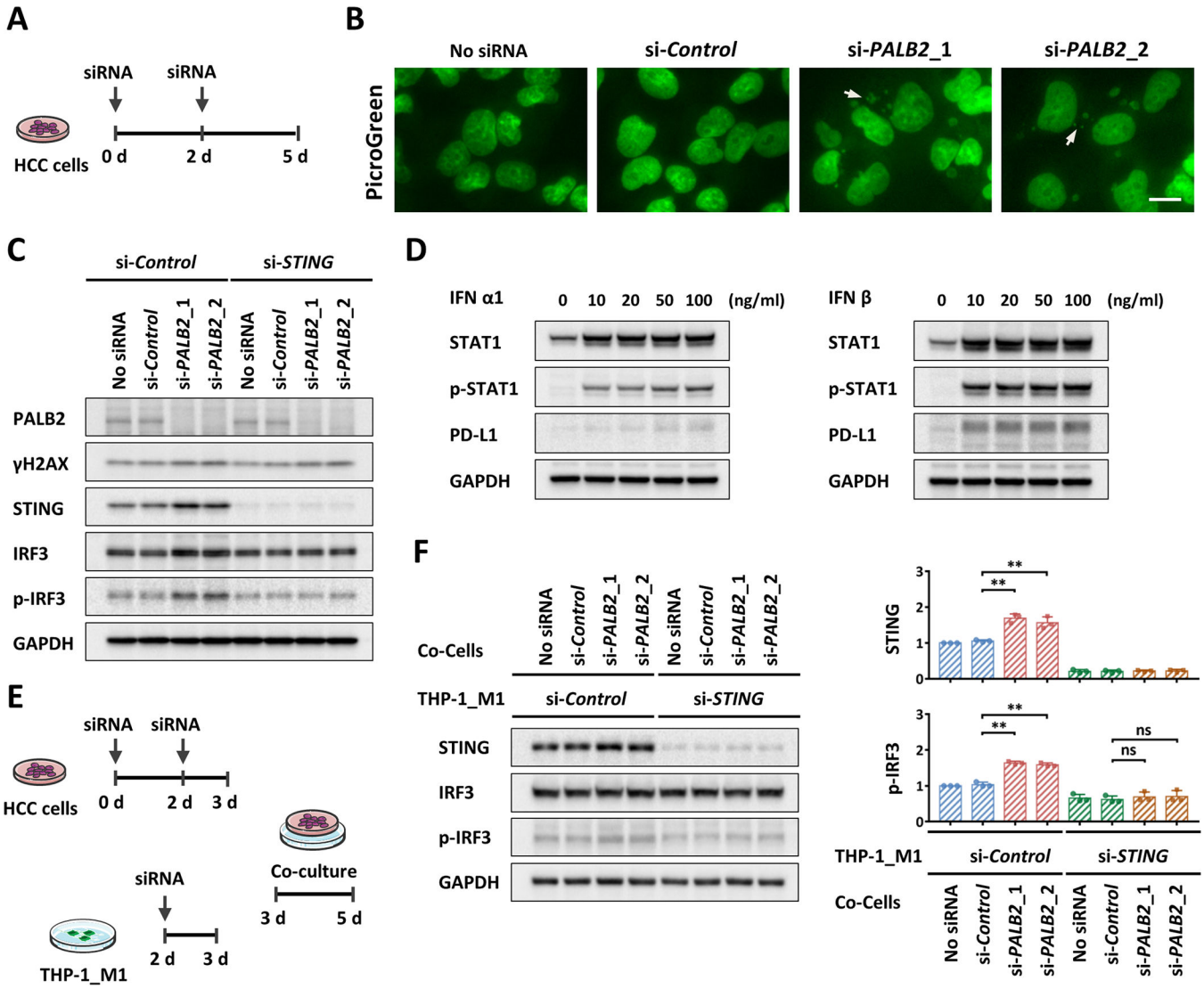

Figure 4. DNA damage induces Type I IFNs through the cGAS-STING pathway in both malignant hepatocytes and M1 macrophages.

(A) Schematic diagram showing the two-step siRNA-mediated knockdown system.

(B) Detection of cytosolic DNA in MHCC97H cells with or without *PALB2* knockdown. DNA was detected using the PicoGreen fluorescence dye selectively binding dsDNA (arrows point to cytosolic DNA; scale bar, 10μm).

(C) Western blots showing higher γH2AX, STING and p-IRF3 levels in LM3 cells with *PALB2* knockdown; no significant difference of p-IRF3 in LM3 cells with *PALB2* and *STING* co-depleted.

(D) Western blots showing that STAT1, p-STAT1 and PD-L1 levels were upregulated in Huh-7 cells after IFNα1 and IFNβ treatment (0, 10, 20, 50, and 100 ng/ml).

(E) Schematic diagram showing the co-culture system of HCC cells and M1 macrophages.

(F) Western blots (left) and quantification of band intensities (right) showing higher STING and p-IRF3 levels in M1 macrophages co-cultured with MHCC97H cells with

Author Manuscript Author Manuscript Author Manuscript Author Manuscript

PALB2 knockdown; no significant difference of p-IRF3 in M1 macrophages with *STING* knockdown co-cultured with HCC cells with *PALB2* depleted.
(***p < 0.01*; mean ± SD)

Author Manuscript Author Manuscript Author Manuscript Author Manuscript

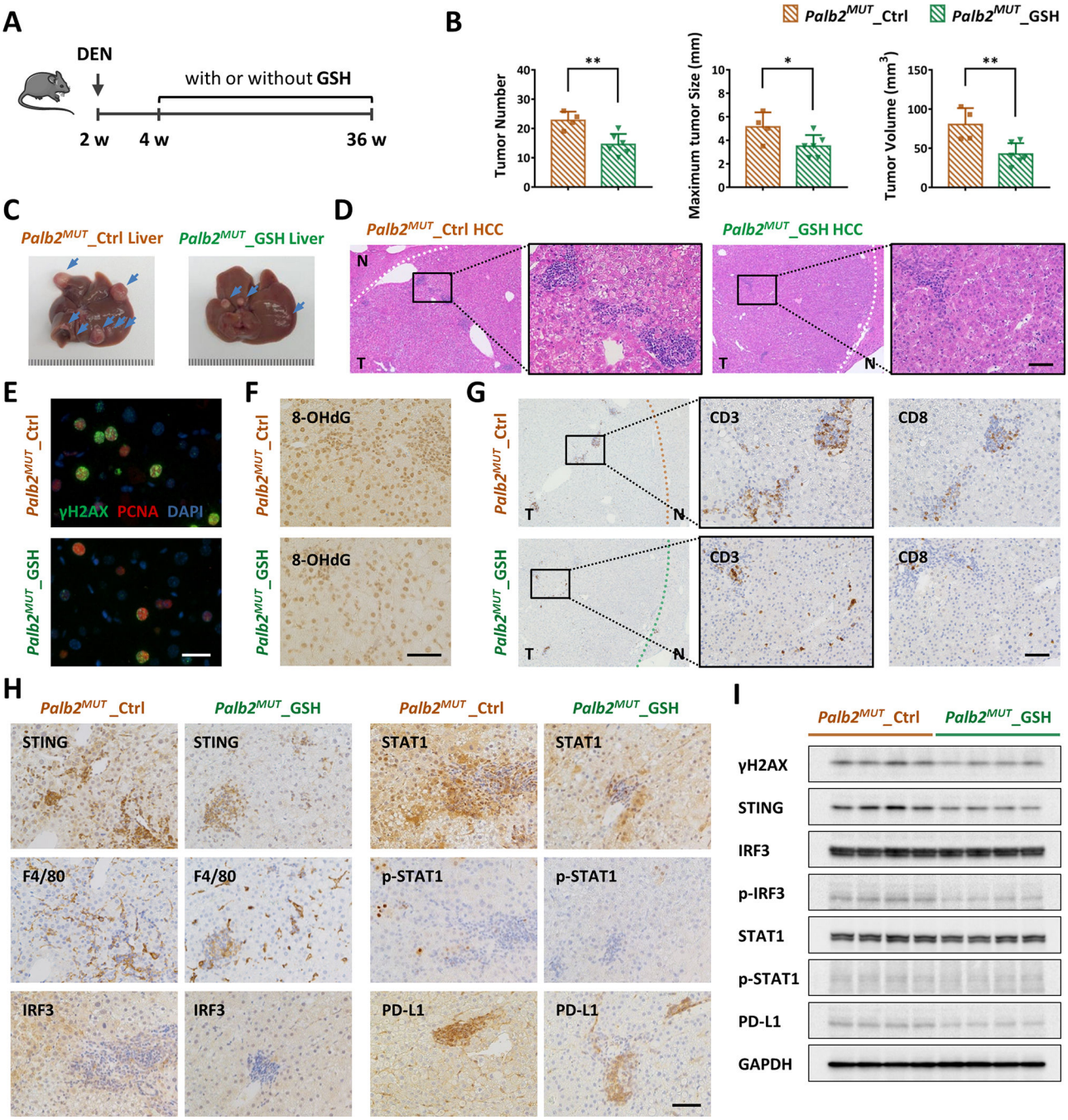

Figure 5. Suppression of oxidative stress alleviates DNA damage and weaken the cGAS-STING signaling pathway in *Palb2*^{MUT} HCC

(A) Schematic diagram showing the DEN-induced HCC model in *Palb2*^{MUT} mice with (n = 6 males, *Palb2*^{MUT}_GSH) or without (n = 4 males, *Palb2*^{MUT}_Ctrl) GSH administration.

(B) Quantification of tumor number, maximum size, and total volume in *Palb2*^{MUT}_Ctrl and *Palb2*^{MUT}_GSH mouse livers. *Palb2*^{MUT}_GSH mouse livers exhibited less tumors, with smaller size and volume.

(C) Representative gross appearance images of *Palb2*^{MUT}_Ctrl and *Palb2*^{MUT}_GSH mouse livers (arrows point to tumors).

Author Manuscript Author Manuscript Author Manuscript Author Manuscript

(D) Representative H&E images showing decreased lymphocyte infiltration in *Palb2*^{MUT}_GSH HCC tumors (T, HCC tumor; N, adjacent normal liver tissue; scale bar, 50 μm).
(E) Representative IF images showing PCNA positive nuclei with less γH2AX foci in *Palb2*^{MUT}_GSH HCC tumors (scale bar, 20 μm).
(F) Representative IHC images showing weaker 8-OHdG nuclear staining in *Palb2*^{MUT}_GSH HCC tumors (scale bar, 50 μm).
(G) Representative IHC images showing less CD3 and CD8-positive lymphocytes infiltrating in *Palb2*^{MUT}_GSH HCC tumors (T, HCC tumor; N, adjacent normal liver tissue; scale bar, 50 μm).
(H) Representative IHC images showing lower STING, IRF3, STAT1, p-STAT1 and PD-L1 levels in *Palb2*^{MUT}_GSH HCC tumors (scale bar, 50 μm).
(I) Western blots showing decreased γH2AX, STING, p-IRF3, STAT1, p-STAT1 and PD-L1 protein levels in *Palb2*^{MUT}_GSH HCC tumors.
(*$p < 0.05$, **$p < 0.01$; mean ± SD)

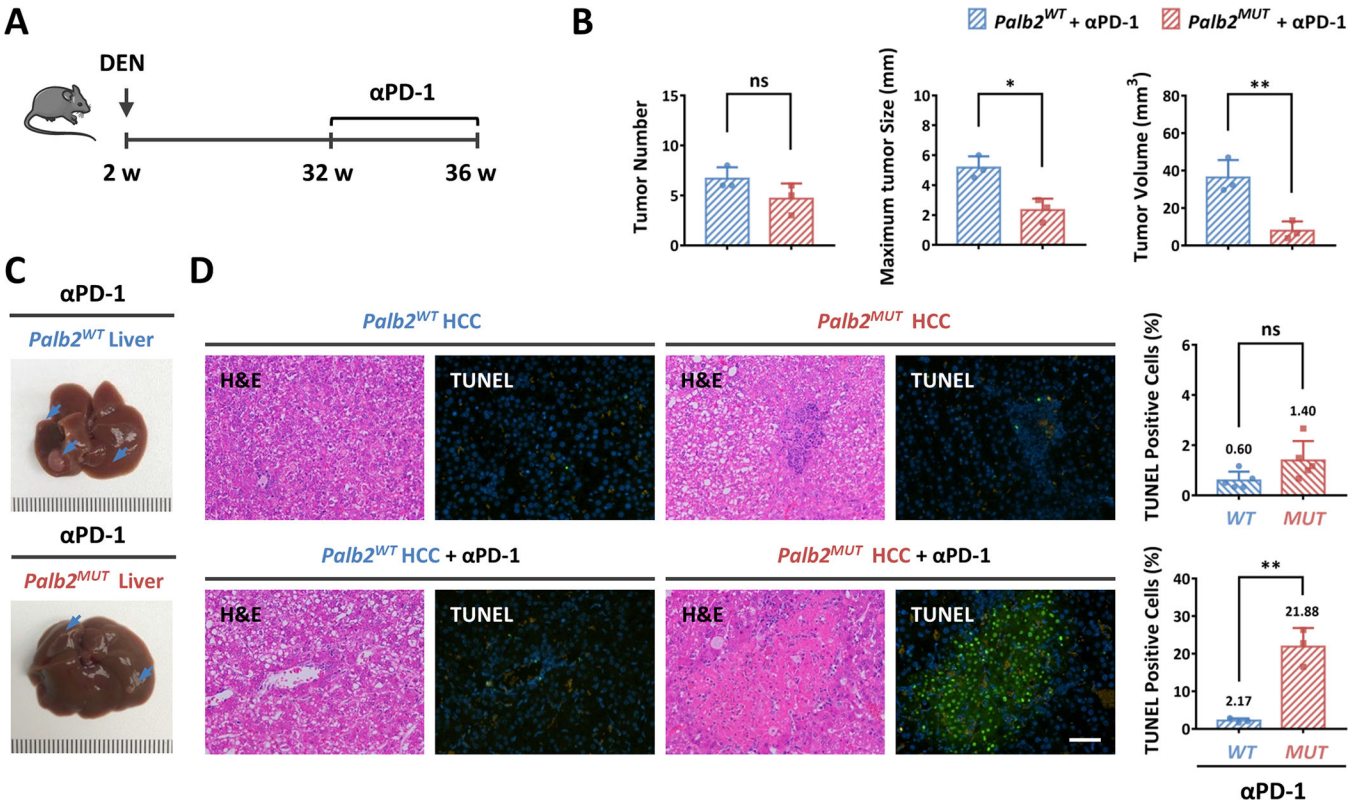

Figure 6. *Palb2*^{MUT} HCC show better response to PD-1 antibody treatment.

(A) Schematic diagram showing the DEN-induced HCC model in *Palb2*^{WT} and *Palb2*^{MUT} mice with PD-1 antibody treatment (n = 3 males per group).

(B) Quantification of tumor number, maximum size and total volume in *Palb2*^{WT} and *Palb2*^{MUT} mouse livers with PD-1 antibody treatment. *Palb2*^{MUT} mouse livers exhibited smaller size and volume tumors.

(C) Representative gross appearance images of *Palb2*^{WT} and *Palb2*^{MUT} mouse livers with PD-1 antibody treatment (arrows point to tumors).

(D) H&E and TUNEL images showing the same part of serial sections. No significant difference in tumor cell death was found between *Palb2*^{WT} and *Palb2*^{MUT} HCC tumors, but *Palb2*^{MUT} HCC tumors with PD-1 antibody treatment exhibited significantly more tumor cell death (mean of each group shown above the column; scale bar, 50 μm).

(*$p < 0.05$, **$p < 0.01$; mean ± SD)

Author Manuscript Author Manuscript Author Manuscript Author Manuscript

Author Manuscript Author Manuscript Author Manuscript Author Manuscript

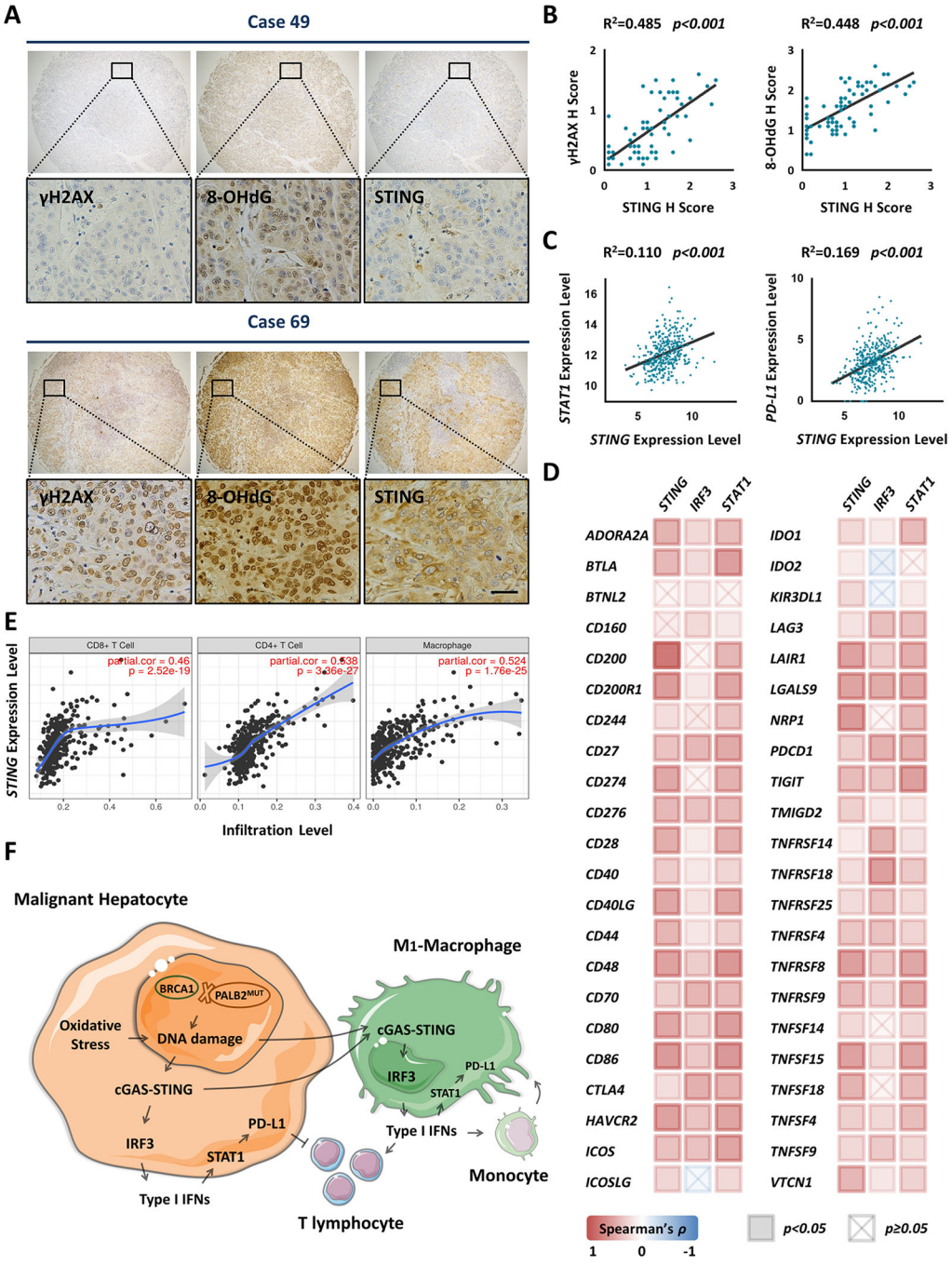

Figure 7. STING expression is associated with DNA damage, and associated with tumor immunosuppression and T-lymphocyte infiltration in human HCC tissues.

(A) Representative IHC images showing low expression (case 49) and high expression (case 69) of γH2AX, 8-OHdG and STING (scale bar, 25μm).

(B) The Pearson correlation analysis between γH2AX level and STING level (left), and between 8-OHdG level and STING level (right) in tumor specimens from 68 patients with HCC.

Author Manuscript Author Manuscript Author Manuscript Author Manuscript

(C) The Pearson correlation analysis between *STING (TMEM173)* and *STAT1* expression (left), and between *STING* and *PD-L1 (CD274)* expression (right) in 371 HCC tissues from TCGA database.

(D) Correlation analysis between *STING*, *IRF3* and *STAT1* expression and 44 common immune checkpoint genes expression in human HCC tissues estimated by TIMER (Spearman's $\rho>0$, positive correlation; Spearman's $\rho<0$, negative correlation).

(E) Correlation analysis between *STING* expression and the infiltration levels of immune cells including $CD4^+$ T cells, $CD8^+$ T cells and macrophages in human HCC tissues estimated by TIMER.

(F) Schematic illustration of HCC immune microenvironment remodelling induced by disrupted BRCA1-PALB2 interaction through cGAS-STING pathway.